Society of Petroleum Engineers

SPE-193660-MS

Pore Scale Simulation of Surfactant Flooding by Lattice Boltzmann Method

Bei Wei, Jian Hou, Dejun Wu, and Huiyu Wang, China University of Petroleum, East China; Hao Liu, China University of Petroleum-Beijing

This paper was prepared for presentation at the SPE International Heavy Oil Conference and Exhibition held in Kuwait City, Kuwait, 10-12 December 2018.

Abstract

Surfactants play an important role in the widely used enhanced heavy oil recovery methods such as surfactant-polymer flooding and alkali-surfactant flooding. In this study, we focus on the effects of surfactant during surfactant flooding and provide a pore scale simulator of surfactant flooding based on the Lattice Boltzmann (LB) method.

We introduce a dipole to present the amphiphilic structure of surfactants in the Lattice Boltzmann model, and characterizes microscopic fluid interactions at the kinetic level. There are three velocity distribution functions to present the oil, water, and surfactant species, and every distribution follows the discrete Boltzmann-BGK equation. There is also an additional dipole vector representing the orientation of amphiphile, so that the interactions related with surfactants depend not only on particle relative distances but also on their dipolar orientations.

The simulation results show that surfactants can reduce the oil-water interfacial tension and recover more oil trapped by capillary force. Moreover, surfactants are able to emulsify the flooding system, forming O/W emulsions or bi-continuous micro-emulsions. Higher surfactant concentration leads to smaller oil droplets in emulsions. In addition, the phase distribution morphologies in porous media are much different in different wetting conditions. By associating the fluid-solid interfacial tension with the surfactants adsorption concentration on walls, we characterize the wettability alteration mechanism in LB model accurately. The oil recovery can be improved by changing the wettability from oil-wet to water wet, increasing the surfactant concentration, and enhancing the adhesion parameters. However, the adsorption onto walls leads to unnecessary waste and could decrease the surfactant concentration in bulk phase.

The study provides an effective pore scale tool to simulate the surfactant involved interfacial flows in porous media. In addition, we can use it to study the flow mechanisms and remaining oil distributions during surfactant flooding.

Keywords: surfactant flooding, Lattice Boltzmann method, emulsification, wettability reversal, heavy oil

INTRODUCTION

Surfactant Flooding is one important enhanced oil recovery (EOR) method, which has been proved able to improve 5%-18% oil recovery in the oilfield development (Dong and Al Yafei, 2015; Lotfollahi et al., 2017), depending on different reservoir types and injection-production parameters. Recently, it is extensively used to develop the heavy oil combined with alkali or polymer (Bryan and Kantzas, 2007; Liu et al., 2006; Yang et al., 2017). In this study, we focus on the surfactant effects in the flooding system. The surfactant possesses both hydrophilic head group and hydrophobic tail group simultaneously. During the surfactant flooding, the head groups tend to enter into aqueous phase and aggregates towards the water, the tail group are apt to combine with oil. In such a way, it reduces the oil-water interfacial tension (IFT) and disperse oil in the solution. In particular, microemulsions formed at a certain surfactant concentration, hydrophilic–lipophilic balance (HLB) number, and water volume fraction, could further promote both mobilization and solubilization of oil. Normally, both physical and chemical adsorption of surfactants occur in the flow through porous media. The surfactants adsorption onto the solid surface may alter the wettability, which could either be more water wet or less water wet, but also leads to surfactant losses inevitably. Therefore, the main mechanisms of surfactant flooding include interfacial tension (IFT) reduction, emulsification, and wettability alteration (Hirasaki et al., 2011).

The surfactant flooding involves complex physiochemical processes including oil-water multiphase flow, convection–diffusion of surfactants, adsorption kinetics on a deforming interface and the solid matrix. Therefore, it is still a challenging work to simulate the surfactant flooding at pore scale. There are three typical pore scale methods can simulate the surfactant flooding processes, namely the pore network, conventional N-S solvers and Lattice Boltzmann method. The pore network describe the pore space as a network and the flow equations following Hagen-poiseuille's law (Blunt, 2001). The advantage of the pore network is its calculating speed; however, it loses local flow details and cannot capture the surfactant features from micro-scale. (Bo et al., 2003) calculated the relative permeability of different chemical flooding use a dynamic pore network, in which they merely characterized the surfactants effects by changing the IFT in different simulations. We can also simulate the flow directly based on the pore-space image by using numerical Stokes solvers or Lattice Boltzmann (LB) method (Ahmed et al., 2017; Raeini et al., 2012). The N-S solvers is based on the conventional Navier-Stokes equations and can be divided into two categories, i.e., interface tracking and interface capturing methods. In those methods, we have to track the interface and it is hard to handle complex porous media boundaries. The popular N-S solvers concerning interfacial flow with surfactants include the boundary integral method (Stone, 1990; Stone and Leal, 1990), front-tracking method (Muradoglu and Tryggvason, 2008), immersed boundary method (Lai et al., 2008), volume-of-fluid (VOF) method (James and Lowengrub, 2004), level-set method (Xu et al., 2012), and phase-field method (Erik Teigen et al., 2011).

In the 21st century, the Lattice Boltzmann method (LBM) has become a popular and efficient tool to model interfacial phenomena in multiphase and multicomponent flows (Wei et al., 2018). It has been widely used in the field of oil and gas exploration, such as the two-phase flow through porous media (Pan et al., 2004), proppant embedment (Fan et al., 2018), shale gas adsorption (Xu et al., 2018), and droplet dynamics with the presence of surfactants (van der Sman and van der Graaf, 2006). The surfactants flooding LB model must be developed based on a LB multicomponent multiphase (MCMP) model, such as the pseudo-potential (Shan-Chen) model (Shan and Chen, 1993), the color-gradient model (Gunstensen et al., 1991), and the free-energy-based model (Swift et al., 1996) et al. The earliest LB models of amphiphilic fluids are free-energy-based multiphase model (Lamura et al., 1998; Lamura et al., 1999; Theissen et al., 1998); however, these models are the so-called ‘top-down’ models, which are more like using a LB scheme ‘clothes’ to solve the interfacial flows combined with the phase-field method and free energy theory. Meanwhile, the color-gradient model is often used solve the multiphase flow in a hybrid surfactant method, in which the surfactant transport equation is solved by another scheme using finite difference method (Liu et al., 2018). In this

study, we used the "bottom-up" LB model proposed by (Chen et al., 2000) to simulate the surfactant flooding process, in which one additional dipole vector is introduced to represent the orientation of amphiphile in this model. It characterizes the microscopic fluid interactions at the kinetic level and the macro performance of the amphiphilic fluids present consequently. We firstly introduce the surfactant LB model, then we show how the model are able to reflect the mechanisms including interfacial tension (IFT) reduction, emulsification, and wettability alteration with simulation results. Finally, we simulate the surfactant flooding process in a pseudo 2D porous medium and analyze the remaining oil types.

MODEL DESCRIPTION

We introduce a dipole to present the amphiphilic structure of surfactants, the schematic and interactions between different components is shown in Figure 1.

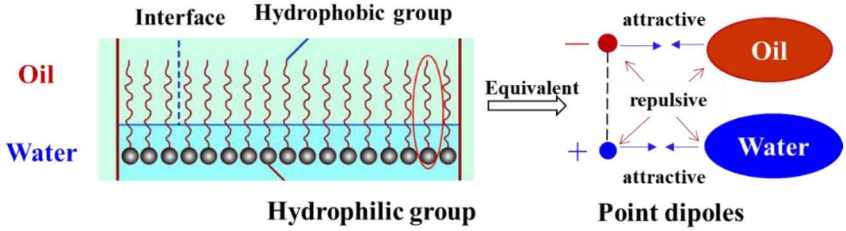

Figure 1—Equivalent simplification of dipoles and amphiphilic structure

In the LB model, there are three velocity distribution functions to present the oil, water, and surfactant species, and every distribution follows the discrete Boltzmann-BGK equation,

$$f_i(\mathbf{x}+\mathbf{e}_i\Delta t, t+\Delta t) = f_i(\mathbf{x},t) - \frac{1}{\tau}(f_i(\mathbf{x},t) - f_i^{eq}(\mathbf{x},t)), \tag{1}$$

where $f_i(x, t)$ is the distribution function, $\mathbf{x}$ is the spatial position, e_i is the discrete velocity, τ is the relaxation time, and $f_i^{eq}(\mathbf{x},t)$ is the equilibrium distribution function. The macroscopic density and macroscopic velocity vector can be calculated from $\rho = \sum_i f_i$, and $\mathbf{u} = \frac{1}{\rho}\sum_i f_i \mathbf{e}_i$, respectively. We use the two-dimensional nine-velocity model (D2Q9) in this study.

The interactions between different components are calculated by pseudo-potential in the Shan-Chen multiphase model. Non-local interactions between fluid particles are incorporated via the following fluid-fluid interaction force,

$$\mathbf{F}_{\text{int},\sigma\sigma'}(\mathbf{x},t) = -\rho_\sigma(\mathbf{x},t) G_{\text{int},\sigma\sigma'} \sum_i \omega_i \rho_{\sigma'}(\mathbf{x}+\mathbf{e}_i\Delta t, t)\mathbf{e}_i, \tag{2}$$

where $G_{\text{int},\sigma\sigma'}$ is a parameter that controls the interaction force strength between different solvent components.

The solid surface force on the σth component can be computed as follows,

$$\mathbf{F}_{\text{ads},\sigma}(\mathbf{x},t) = -G_{\text{ads},\sigma}\rho_\sigma(\mathbf{x},t)\sum_i \omega_i s(\mathbf{x}+\mathbf{e}_i\Delta t, t)\mathbf{e}_i, \tag{3}$$

where the $s(\mathbf{x} + \mathbf{e}_i\Delta t,t)$ is an indicator function for a solid or fluid domain node, $G_{\text{ads},\sigma}$ is the wall adhesion parameter.

There is also an additional dipole vector $\mathbf{d}(\mathbf{x}, t)$ which represents the orientation of amphiphile satisfies a BGK-like process,

$$\rho_s(\mathbf{x},t+\Delta t)\mathbf{d}(\mathbf{x},t+\Delta t) = \sum_i f_{s,i}(\mathbf{x}-\mathbf{e}_i\Delta t, t)\bar{\mathbf{d}}(\mathbf{x}-\mathbf{e}_i\Delta t, t), \tag{4}$$

where $\bar{\mathbf{d}}$ represents the post-colllision average dipole vector which follows,

$$\bar{\mathbf{d}}(\mathbf{x},t)=\mathbf{d}(\mathbf{x},t)-\frac{1}{\tau_d}[\mathbf{d}(\mathbf{x},t)-\mathbf{d}^{eq}(\mathbf{x},t)]. \tag{5}$$

where τ_d is the relaxation time of the dipole vector, and the equilibrium orientation $\mathbf{d}^{eq}$ is derived from a mean field approach.

The interactions related with surfactants include the force acting on the solvent particles due to amphiphilic dipoles $F_{int,\sigma s}$, the force acting on amphiphilic molecules due to solvent particles $F_{int,s\sigma}$, and the force among surfactant molecules $F_{int,ss}$. These interactions are given by

$$\mathbf{F}_{\text{int},\sigma s}(\mathbf{x},t)=-2\rho_\sigma(\mathbf{x},t)G_{\text{int},\sigma s}\sum_{i\neq 0}\mathbf{d}(\mathbf{x}+\mathbf{e}_i\Delta t,t)\cdot\boldsymbol{\theta}_i\rho_s(\mathbf{x}+\mathbf{e}_i\Delta t,t), \tag{6}$$

$$\mathbf{F}_{\text{int},s\sigma}(\mathbf{x},t)=2\rho_s(\mathbf{x},t)\mathbf{d}(\mathbf{x},t)\sum_{\sigma}G_{\text{int},\sigma s}\sum_{i\neq 0}\boldsymbol{\theta}_i\rho_\sigma(\mathbf{x}+\mathbf{e}_i\Delta t,t), \tag{7}$$

$$\begin{aligned}\mathbf{F}_{\text{int},ss}(\mathbf{x},t)=-\frac{4D}{c^2}G_{\text{int},ss}\rho_s(\mathbf{x},t)\sum_{i\neq 0}\rho_s(\mathbf{x},t)\{&\mathbf{d}(\mathbf{x}+\mathbf{e}_i\Delta t,t)\mathbf{d}(\mathbf{x},t):\boldsymbol{\theta}_i\mathbf{e}_i\\&+[\mathbf{d}(\mathbf{x}+\mathbf{e}_i\Delta t,t)\mathbf{d}(\mathbf{x},t)+\mathbf{d}(\mathbf{x},t)\mathbf{d}(\mathbf{x}+\mathbf{e}_i\Delta t,t)]\cdot\mathbf{e}_i\}.\end{aligned} \tag{8}$$

where $G_{\text{int},\sigma s}$ and $G_{\text{int},ss}$ are the interaction force parameters that control the strength between the solvent component and surfactant molecules, and the strength among surfactant molecules, respectively.

Results and Discussion

Unless stated specially, we use a set of basic parameters throughout the simulations to ensure the numerical stability. The parameters are set as D=2, $\tau_o = \tau_w = \tau_s = 1$, $\tau_d = 1.2$, $G_{\text{int,ow}} = 2.1$, $G_{\text{int,ws}} = -G_{\text{int},os} = -0.1$, and $G_{\text{int},ss} = -0.2$.

Interfacial tension reduction

We set a series oil droplet with the radius of 25 lattice in the water, and calculated the oil-water IFT by Laplace's law at different concentrations of surfactant, as shown in Figure 2. The IFT decreases with surfactant concentration more and more quickly. Moreover, it reach at an ultra-low IFT state when the concentration is higher than 35%. What should be explained is that the concentration in the LB model is not the real concentration in the oil displacement system, their relation can be fitted according to the IFT reduction degree. Figure 3 shows the capillary fingering phenomena at different surfactant concentration and time step (ts). The inlet and outlet are applied with Zou-He pressure boundaries and the solid walls are applied with bounce-back boundaries. The initial porous media are full of oil and the capillary force is dominant during the flow. The displacing front becomes more homogeneous and move faster with the surfactant increase. This is because the surfactant decreases the IFT and recover the oil trapped in pores, consequently inhibit the capillary fingering.

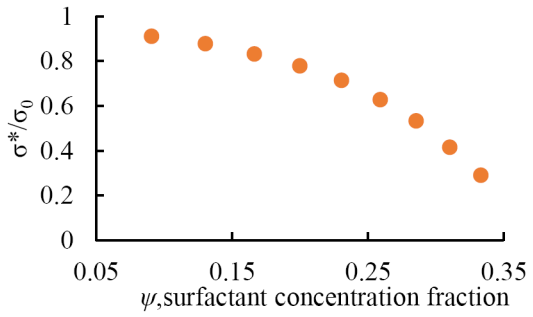

Figure 2—IFT at different surfactant concentrations in LB model, σ0 is the initial IFT without surfactant; σ* is the interfacial tension with surfactant cover.

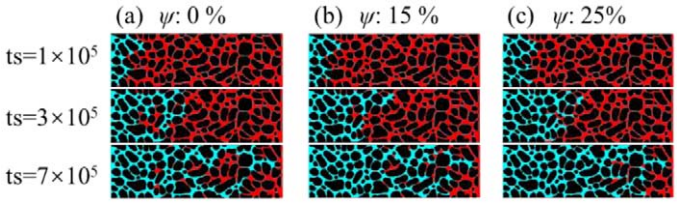

Figure 3—Capillary fingering in surfactant flooding with different surfactant concentrations, the red, cyan, and black represents oil, water, and solid rock, respectively.

Emulsification

We simulate the phase separation process by setting the oil-water fraction ratio as 0.6:0.4 at a 100×100 domain randomly. Figure 4 shows the pure oil-water phase separation result and binary system phase separation with the surfactant concentration of 16% at 50000 time step. The experiment configurations of heavy oil droplets in pure water and water containing surfactants are also given along with the simulation results as a comparison. We can see that the surfactants inhibit the coalescence of oil droplet and form O/W emulsions. The experiment configurations are consistent with the simulations. Thus the LB model can capture the emulsification effects accurately. Increasing the surfactant concentration to 30%, we can further obtain the bi-continuous micro-emulsion, as shown in Figure 5.

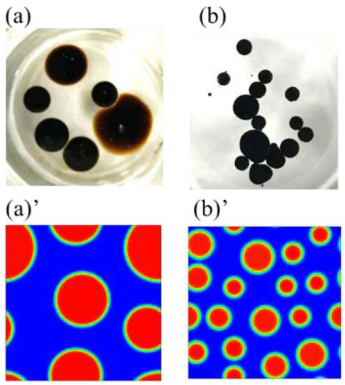

Figure 4—Phase separation of oil-water system, the red represents the oil and the blue is water. (a) oil droplets in pure water (b) oil droplets in water containing surfactant (a)' LB simulation of phase separation of oil-water binary system (b)' LB simulation of phase separation in oil-water-surfactant ternary system.

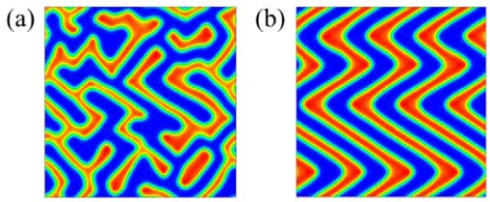

Figure 5—Bi-continuous micro-emulsion during phase separation of oil-water-surfactant ternary system. (a) the initial density distribution is random (b) the initial density distribution is like zebra-stripe

To investigate the phase behavior in porous media, we simulate the phase separation in a CT image of sandstone from Shengli Oilfield. Two set of parameters are used to achieve different wetting conditions, i.e., $G_{ads,w} = 0.1$, $G_{ads,o} = 0.6$, and $G_{ads,s} = 0$, to specify intrinsic contact angle of the oil droplet as 108° on water-wet walls, and the intrinsic contact angle is 63° for oil wet condition when $G_{ads,w} = 0.1$, $G_{ads,o} = -0.2$, and $G_{ads,s} = 0$. Phase distribution in porous media under different wetting conditions, oil saturations and surfactant concentrations are shown in Figure 6. It shows that the oil tend to adsorb onto walls in oil-wet porous media while the oil are able to disperse in pore space in water-wet condition. The surfactants emulsify the oil to O/W emulsions or bi-continuous phase emulsion, which enhance the oil deformability and decrease the flow resistance.

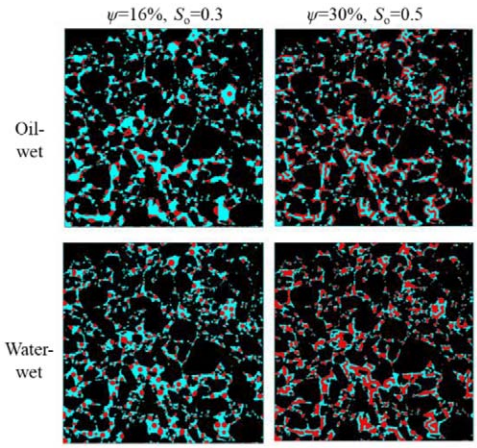

Figure 6—Phase distribution in porous media under different wetting conditions, oil saturations and surfactant concentrations.

Wettability alteration

During the surfactant flooding process, surfactants are apt to adsorb on walls, and then alter the wettability. To characterize this feature, we need make clear how the wetting conditions work in Shan-Chen LB models. According to Young's relation:

$$\cos\theta_o = \frac{\sigma_{sw} - \sigma_{so}}{\sigma_{ow}} \tag{9}$$

where σ_{ow},σ_{sw} and σ_{so} are the IFT of fluid interface and the fluid–solid interfaces respectively. In the previous model, surfactants only decrease the IFT of fluid interface so the absolute value of the Cosine function increases. When the contact angle of clean oil droplet is less than 90°, the value of $\cos\theta_o$ is positive and increases with the presence of surfactants, leading to a smaller contact angle. In contrast, in the case of the contact angle larger than 90°, the value of $\cos\theta_o$ is negative and decreases with the presence of surfactants, resulting in the increase of the contact angle. Therefore, there no chance to reverse the wettability in the previous model. As the IFT of fluid–solid interfaces are proportional to the solid adhesion parameters, we can control the wettability by changing $G_{ads,w}$ and $G_{ads,o}$ according to the local surfactants concentration on

walls. Here we only give an example to realize the wettability reversal from the oil-wet to water-wet by changing $G_{ads,w}$

$$G_{ads,w} = G_{ads,wi} + k_1 \psi_{wall} \ln(1 + k_2 G_{ads3,s}), \quad (10)$$

where $G_{ads,wi} = 0.1$ is the water adhesion parameter for the clean wall with no surfactant adsorption, k_1 and k_2 are constant coefficients, and $G_{ads3,s}$ is no longer equal to 0 if we consider the surfactants adsorption. Figure 7 gives the phase distribution configurations and surfactant concentration profile when k_1=10, k_2=0.5, and $G_{ads3,s}$ = −0.5 at the beginning of the surfactant flooding. It shows that the oil on the left of the yellow line, i.e., the area that have been swept by surfactants, is water-wet, while the right oil droplets is oil-wet. In addition, the surfactants mainly aggregate on the fluid-fluid interface and walls. This is because the surfactants adsorbed on walls alter the wettability.

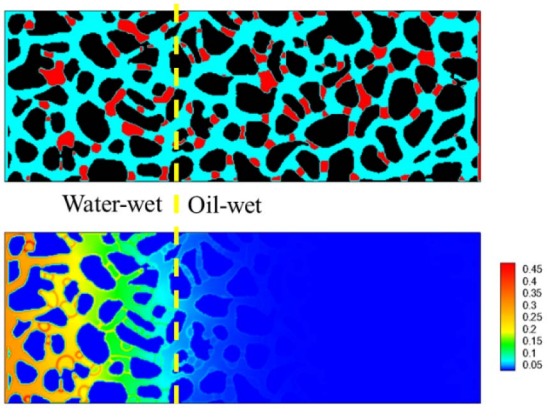

Figure 7—Phase distribution configurations and surfactant concentration profile at the beginning of the surfactant flooding.

Application in surfactant flooding

We simulate the surfactant flooding in the porous media with residual oil saturation of 0.3. The oil distribution is uniform in the porous media and Zou-He pressure boundaries are applied in the inlet and outlet. Figure 8 shows the water saturation evolution along with time under different wetting conditions, surfactant concentrations, and adsorption strengths. The oil recovery is improved by changing the wettability from oil-wet to water wet, increasing the surfactant concentration, and enhancing the adhesion parameters. However, it does not means the stronger the adhesion parameters the better, because the surfactant adsorption onto walls leads to inevitable loss and can decrease the surfactant concentration in bulk phase, consequently weaken the IFT reduction effect of surfactants. That's why the case with adhesion parameter of −0.4 has larger oil recovery than that with −0.6 in Figure 8.

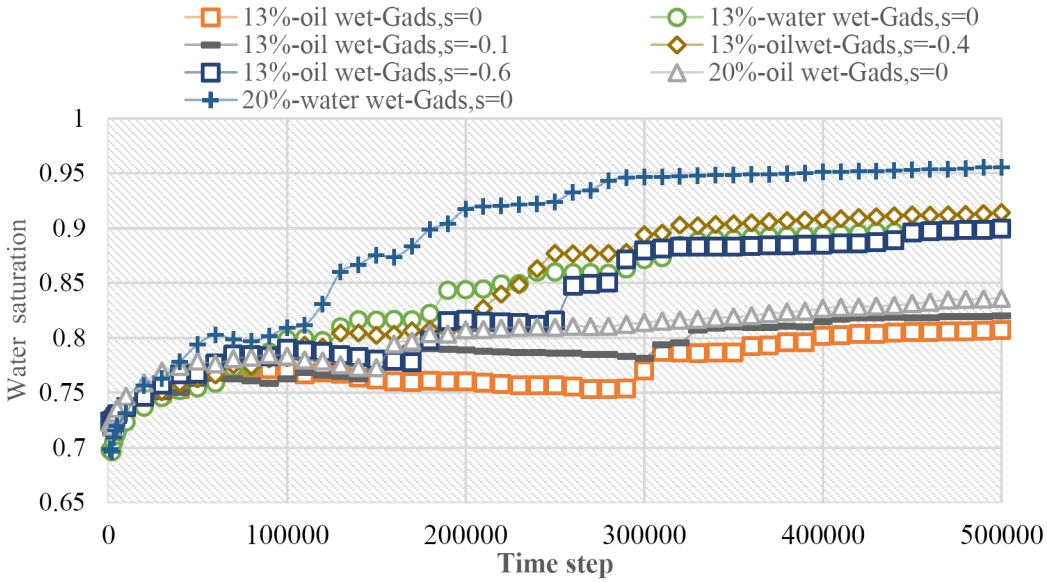

Figure 8—Water saturation evolution during the surfactant flooding, Gads,s=0 means there are no surfactants adsorbed on walls, and the larger of the absolute value of Gads,s, the stronger of the adsorption strength.

We further classify the remaining oil distributions during surfactant flooding at quasi-steady state into a few groups: (1) Oil films adhere to the solid surface, (2) Oil pools occupy multiple pore bodies, (3) Oil trapped in dead ends, (4) Oil droplets trapped by Jamin effect, (5) Oil bridges between throats, and (6) hidden oil on the down-gradient side of walls. And these patterns are show in Figure 9, marked with the number as stated above. Moreover, these types are not monotonous and may transform from one type to another along with the flow. In particular, the surfactant-laden oil perform better deformability and is easier to snap off in pores, which contribute to the formation of hidden oil on the down-gradient side of walls. In addition, the formation of hidden oil is also related to the local flow field, Figure 10 give four examples in different wetting conditions. It is easy to recover this type oil by changing the gradient direction of flow field periodically.

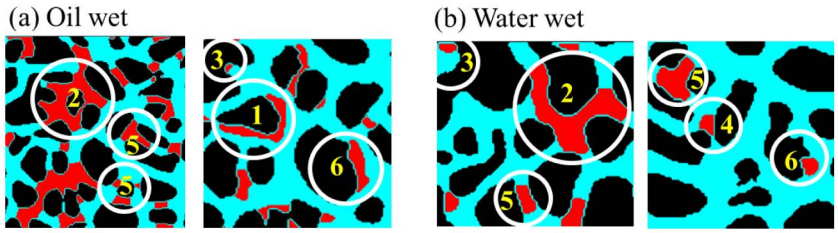

Figure 9—Different remaining oil types

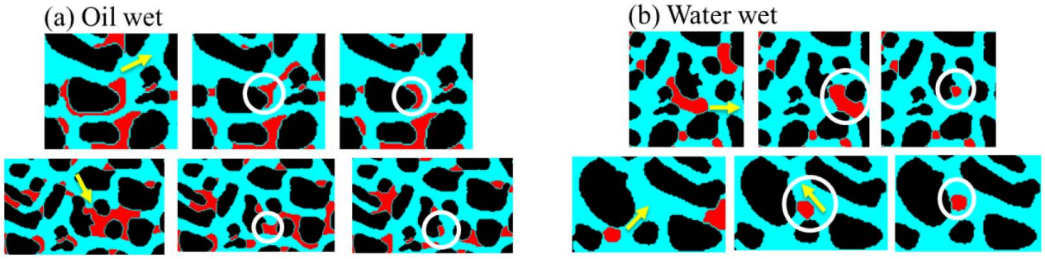

Figure 10—Hidden oil on the down-gradient side of walls

Conclusion

To sum up, we improved the surfactant Lattice Boltzmann model so that the flow characteristics during surfactant flooding, such as the interfacial tension reduction, emulsification, and wettability alteration, can be considered. First, surfactants can reduce the IFT and recover more oil trapped by capillary force. Moreover, surfactants are able to emulsify the flooding system, forming O/W emulsions or bi-continuous micro-emulsions. The oil phase are apt to adsorb on solid walls in oil-wet porous media. Furthermore, we associate the surfactant adsorption strength with the wetting conditions to realize the wettability reversal. Finally, the surfactant flooding simulation results show that oil recovery is improved with the presence of surfactants; however, it doesn't mean the more surfactants adsorbed on walls the better, for the adsorption onto walls leads to unnecessary waste and could decrease the surfactant concentration in bulk phase. There is also one remaining oil type worthy to note, which is called hidden oil on the down-gradient side of walls in this paper, that it is easy to recover the oil by changing the gradient direction of flow field periodically.

Acknowledgement

The wrok is supported by the following projects: National Natural Science Foundation of China (51574269), the National Science Foundation for Distinguished Young Scholars of China (51625403).

References

Ahmed, K. et al., 2017. Characterizing Unconsolidated Heavy Oil Sands Using Cryogenic MicroCT - A Pilot Study from Kuwait, SPE Canada Heavy Oil Technical Conference. *Society of Petroleum Engineers*, Calgary, Alberta, Canada, SPE-184979-MS.

Blunt, M.J., 2001. Flow in porous media—pore-network models and multiphase flow. *Current opinion in colloid & interface science*, **6**(3): 197–207.

Bo, Q., Zhong, T. and Liu, Q., 2003. Pore Scale Network Modeling of Relative permeability in Chemical flooding, SPE International Improved Oil Recovery Conference in Asia Pacific. *Society of Petroleum Engineers*, Kuala Lumpur, Malaysia, SPE-84906-MS.

Bryan, J.L. and Kantzas, A., 2007. Enhanced Heavy-Oil Recovery by Alkali-Surfactant Flooding, SPE Annual Technical Conference and Exhibition. *Society of Petroleum Engineers*, Anaheim, California, USA, SPE-110738-MS.

Chen, H., Boghosian, B.M., Coveney, P.V. and Nekovee, M., 2000. A ternary lattice Boltzmann model for amphiphilic fluids. Proceedings of the Royal Society A: Mathematical, Physical and Engineering Sciences, **456**(2000): 2043–2057.

Dong, H. and Al Yafei, A., 2015. Optimization of Surfactant Flooding for Carbonate Reservoirs, Abu Dhabi International Petroleum Exhibition and Conference. *Society of Petroleum Engineers*, Abu Dhabi, UAE, SPE-177489-MS.

Erik Teigen, K., Song, P., Lowengrub, J. and Voigt, A., 2011. A diffuse-interface method for two-phase flows with soluble surfactants. *Journal of Computational Physics*, **230**(2): 375–393.

Fan, M. et al., 2018. Investigating the Impact of Proppant Embedment and Compaction on Fracture Conductivity Using a Continuum Mechanics, DEM, and LBM Coupled Approach, 52nd U.S. Rock Mechanics/Geomechanics Symposium. American Rock Mechanics Association, Seattle, Washington.

Gunstensen, A.K., Rothman, D.H., Zaleski, S. and Zanetti, G., 1991. Lattice Boltzmann model of immiscible fluids. *Physical Review A*, **43**(8): 4320.

Hirasaki, G.J., Miller, C.A. and Puerto, M., 2011. Recent Advances in Surfactant EOR. *SPE JOURNAL*, **16**(4): 889–907.

James, A.J. and Lowengrub, J., 2004. A surfactant-conserving volume-of-fluid method for interfacial flows with insoluble surfactant. *Journal of Computational Physics*, **201**(2): 685–722.

Lai, M., Tseng, Y. and Huang, H., 2008. An immersed boundary method for interfacial flows with insoluble surfactant. *Journal of Computational Physics*, **227**(15): 7279–7293.

Lamura, A., Gonnella, G. and Yeomans, J.M., 1998. Modeling the Dynamics of Amphiphilic Fluids. *International Journal of Modern Physics C*, **09**(08): 1469–1478.

Lamura, A., Gonnella, G. and Yeomans, J.M., 1999. A lattice Boltzmann model of ternary fluid mixtures. *Europhysics Letters*, **45**(3): 314 - 320.

Liu, H. et al., 2018. A hybrid lattice Boltzmann and finite difference method for droplet dynamics with insoluble surfactants. *Journal of Fluid Mechanics*, **837**: 381–412.

Liu, Q., Dong, M. and Ma, S., 2006. Alkaline/Surfactant Flood Potential in Western Canadian Heavy Oil Reservoirs, SPE/DOE Symposium on Improved Oil Recovery. *Society of Petroleum Engineers*, Tulsa, Oklahoma, USA, SPE-99791-MS.

Lotfollahi, M. et al., 2017. Optimization of Surfactant Flooding in Tight Oil Reservoirs, SPE/AAPG/SEG Unconventional Resources Technology Conference. Unconventional Resources Technology Conference, Austin, Texas, USA, URTEC-2696038-MS.

Muradoglu, M. and Tryggvason, G., 2008. A front-tracking method for computation of interfacial flows with soluble surfactants. *Journal of Computational Physics*, **227**(4): 2238–2262.

Pan, C., Hilpert, M. and Miller, C.T., 2004. Lattice-Boltzmann simulation of two-phase flow in porous media. *Water Resources Research*, **40**(1).

Raeini, A.Q., Blunt, M.J. and Bijeljic, B., 2012. Modelling two-phase flow in porous media at the pore scale using the volume-of-fluid method. *Journal of Computational Physics*, **231**(17): 5653–5668.

Shan, X. and Chen, H., 1993. Lattice Boltzmann model for simulating flows with multiple phases and components. *Physical Review E*, **47**(3): 1815.

Stone, H.A., 1990. A simple derivation of the time-dependent convective-diffusion equation for surfactant transport along a deforming interface. *Physics of Fluids A: Fluid Dynamics*, **2**(1): 111–112.

Stone, H.A. and Leal, L.G., 1990. The effects of surfactants on drop deformation and breakup. *Journal of Fluid Mechanics*, **220**(-1): 161.

Swift, M.R., Orlandini, E., Osborn, W.R. and Yeomans, J.M., 1996. Lattice Boltzmann simulations of liquid-gas and binary fluid systems. *Physical Review E*, **54**(5): 5041.

Theissen, O., Gompper, G. and Kroll, D.M., 1998. Lattice-Boltzmann model of amphiphilic systems. *Europhysics Letters*, **42**(4): 419 - 424.

van der Sman, R.G.M. and van der Graaf, S., 2006. Diffuse interface model of surfactant adsorption onto flat and droplet interfaces. *Rheologica Acta*, **46**(1): 3–11.

Wei, B., Huang, H., Hou, J. and Sukop, M.C., 2018. Study on the meniscus-induced motion of droplets and bubbles by a three-phase Lattice Boltzmann model. *Chemical Engineering Science*, **176**: 35–49.

Xu, J., Yang, Y. and Lowengrub, J., 2012. A level-set continuum method for two-phase flows with insoluble surfactant. *Journal of Computational Physics*, **231**(17): 5897–5909.

Xu, R., Prodanovi, C., Ma, S., A and Landry, C.J., 2018. Simulation of Gas Adsorption and Capillary Condensation in Shale Nanopores Using Lattice Boltzmann Modeling, SPE/AAPG/SEG Unconventional Resources Technology Conference. Unconventional Resources Technology Conference, Houston, Texas, USA, URTEC-2902821-MS.

Yang, Y. et al., 2017. New Composite Viscosity Reducer with Both Asphaltene Dispersion and Emulsifying Capability for Heavy and Ultraheavy Crude Oils. *Energy & Fuels*, **31**(2): 1159–1173.